

**Fundamentals of Soft Thermofluidic System Design**

Journal:	<i>Soft Matter</i>
Manuscript ID	SM-ART-03-2020-000504.R1
Article Type:	Paper
Date Submitted by the Author:	24-Jun-2020
Complete List of Authors:	Kotagama, Praveen; Arizona State University, School for Engineering of Matter, Transport and Energy Manning, Kenneth; Arizona State University, School for Engineering of Matter, Transport and Energy Rykaczewski, Konrad; Arizona State University, School for Engineering of Matter, Transport and Energy

Fundamentals of Soft Thermofluidic System Design

Praveen Kotagama^a, Kenneth C. Manning^a, and Konrad Rykaczewski^{a,*}

- a. School for Engineering of Matter, Transport and Energy, Arizona State University,
Tempe, AZ 85287, USA. Email: konradr@asu.edu

The soft composition of many natural thermofluidic systems allows them to effectively move heat and control its transfer rate by dynamically changing shape (e.g. dilation or constriction of capillaries near our skin). So far, making analogous deformable “soft thermofluidic systems” has been limited by the low thermal conductivity of materials with suitable mechanical properties. By remaining soft and stretchable despite the addition of filler, elastomer composites with thermal conductivity enhanced by liquid-metal micro-droplets provide an ideal material for this application. In this work, we use these materials to develop an elementary thermofluidic system consisting of a soft, heat generating pipe that is internally cooled with flow of water and explore its thermal behavior as it undergoes large shape change. The transient device shape change invalidates many conventional assumptions employed in thermal design making analysis of this devices’ operation a non-trivial undertaking. To this end, using time scale analysis we demonstrate when the conventional assumptions break down and highlight conditions under which the quasi-static assumption is applicable. In this gradual shape modulation regime the actuated devices’ thermal behavior at a given stretch approaches that of a static device with equivalent geometry. We validate this time scale analysis by experimentally characterizing thermo-fluidic behavior of our soft system as it undergoes axial periodic extension-retraction at varying frequencies during operation. By doing so we explore multiple shape modulation regimes and provide a theoretical foundation to be used in the design of soft thermofluidic systems undergoing transient deformation.

Introduction

From building-sized power plant condensers to fingertip-sized microelectronics cooling systems,¹ thermofluidic systems are used to transfer thermal energy in an immense array of applications. Since at least the industrial revolution, such systems have been made of rigid, predominantly metallic materials; as a result, the design knobs that we can manipulate for operational control are limited to the flow temperature and rate. In contrast, in nature there are many elegant systems based on soft materials that effectively move heat and control its transfer rate by dynamically changing shape. For example, based on cooling or heating needs of our own bodies, the capillaries near our skin dilate or constrict.² Making of analogous deformable “soft thermofluidic systems” has so far been limited by the lack of multifunctional materials with a fitting set of thermo-mechanical properties. Specifically, traditional synthetic soft materials with suitable mechanical properties have a thermal conductivity ($k \approx 0.2 \text{ Wm}^{-1}\text{K}^{-1}$) that is too low for most industrial applications.

The lack of effective materials for soft thermofluidic systems is beginning to be addressed with the recent introduction of elastomer composites with room-temperature liquid metal (LM) fillers.^{3–6} In contrast to solid particle fillers, LM micro-droplets deform with the elastomer matrix which drastically reduces the impact on a composite’s mechanical properties. These materials have shown up to 600% extensibility even with 50% of the composite volume being occupied by liquid metal.⁴ At the same time, adding LM increases thermal conductivity up to 2 to 5 $\text{Wm}^{-1}\text{K}^{-1}$ (for filler volume fraction, ϕ , of 50 to 80%) in an undeformed state and up to 10 $\text{Wm}^{-1}\text{K}^{-1}$ anisotropically if the material is stretched (with $\phi = 50\%$).^{4,5} The numerous recent reports of further improvements in thermal conductivity of LM itself^{7,8} and in elastomer-LM composites^{5,9–}

¹¹ achieved through the incorporation of solid particles, indicate that improvements in thermal properties of soft materials are likely to continue.

With this enabling technology in mind, in this work we use LM-elastomer composite to develop an elementary thermofluidic system consisting of a soft, heat generating pipe that is internally cooled with flow of water. We lay the foundations of a theoretical framework for the design of such devices that undergo large shape-change during operation. Such a task is not a trivial undertaking since transient device shape change invalidates many conventional assumptions employed in thermofluidic system analysis^{1,12} including a static diameter, length, and wall thickness as well as constant flow, material properties, and boundary conditions. Using a time scale analysis, we identify conditions under which the quasi-static assumption is applicable. In this gradual shape modulation regime the actuated device thermal behavior at given stretch approaches that of a static device with equivalent geometry. We validate our time scale analysis by experimentally characterizing thermo-fluidic performance of our liquid-cooled heat generating soft pipe as it undergoes axial stretching and retraction during operation.

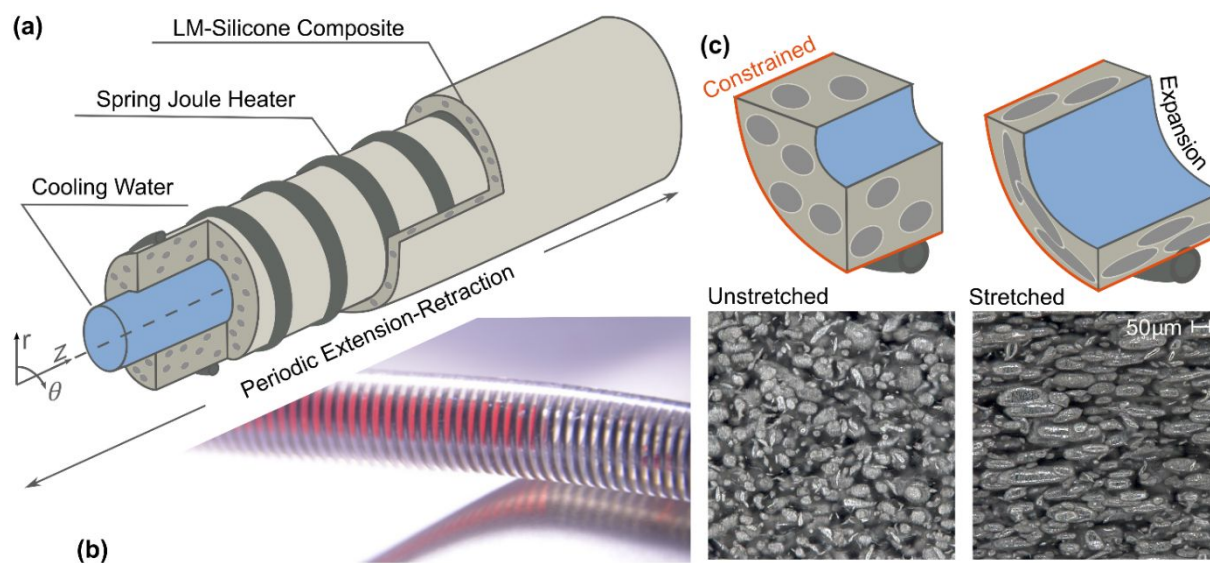


Fig. 1. Illustration (a) and photograph (b) of an example liquid-cooled, heat generating soft pipe; in (b) only silicone was used to make the tube to make the extension spring embedded in the tube wall as well as dyed red water in the inner cavity visible; (c) top row schematically shows the effects of axial extension on the tube wall, inner channel, and the liquid metal micro-droplets; the bottom row shows the microscopic view of the effects of tube stretching on the liquid metal droplets.

Results and Discussion

To begin exploring the novel concept of a soft, stretchable thermofluidic system undergoing large shape change during operation, we fabricated elementary stretchable heat generating tube that is internally cooled with water flow out of silicone with 0% and 20% volume fraction of liquid metal micro-droplets averaging a diameter of $60\ \mu\text{m}$ (see Fig. 1a-c and ESI for further details). As illustrated in Fig. 1c, stretching the tube expands the inner diameter and elongates the LM micro-droplets, resulting in anisotropic thermal properties that need to be considered. The tubes are embedded with steel extension springs to serve both as an extensible joule heater and a resistive temperature probe (see Fig. 1a and 1b). These heated tubes are incorporated as a stretchable section of a carefully designed and calibrated flow loop. We used a linear actuator to continuously stretch and retract the heated soft tube from an initial 15% to a 45% stretch at a constant rate ranging from 0.3 to $8\ \text{mms}^{-1}$. We discuss further details in the Experimental section.

The used geometrical and operational settings allowed us to vary time scales over the range required to validate our analysis and discuss applicability of and deviation from predictions based on the quasi-static shape assumption. By doing so, we set up a guideline on how such transient problems can be approached and how to evaluate the complexity of a soft thermofluidic system

design. Next we discuss the details of the time scale analysis and experimental characterization of the thermal performance of the device used to validate our theoretical notions.

Time scale analysis of the soft thermofluid system

Predictive models based on the quasi-static assumption are often employed to overcome the complications of transient models. These models assume that the time scales of transient effects occur rapidly enough to consider the changes as discrete incremental states that achieve a steady state prior to transitioning to the next state, i.e quasi-static. In order to evaluate the validity and applicability of the quasi-static assumption to a system, we must identify and compare relevant characteristic time scales for the occurring physical processes. For our system, primary modes of heat transfer are conduction across the tube wall and internal forced convection from the tube wall to the water. The characteristic time scale for the conduction of heat across the wall with thickness $h \approx 1$ mm that is composed of material with transverse thermal diffusivity ($\alpha_{wall} \approx 0.13 - 0.34$ mm²s⁻¹) is equal to $t_k = h^2/\alpha_{wall}$ which for our experimental values ranges from 4 to 7 s.¹³ From convection perspective, one possibility for characteristic time can be thought of as the average time taken by a water molecule moving with mean axial velocity ($U \approx 237$ to 190 mms⁻¹) to travel through the tube length (i.e. $t_{c-axial} = L/U$ which for our experimental value ranges from 1 to 2 s). However, since our flow is hydrodynamically but not thermally developed across the entire length of stretched or unstretched tube (see discussion in ESI), the more relevant characteristic convective time scale represent the time for radial diffusion of heat across the local thermal boundary layer thickness ($t_{c-radial} = \delta_T^2/\alpha_{water}$). Based on the solutions to the Graetz problem,¹³ at the exit of our stretched and unstretched tube $\delta_T \approx 0.9 r$ (see details in ESI). As such, we can roughly estimate the average boundary layer thickness across the length of the pipe as $\delta_T/2$, which

by coincidence yields average $t_{c-radial}$ of again 1 of 2 s (i.e. local $t_{c-radial}$ is smaller than this value near entrance leading to $t_{c-radial} < t_k$ but is larger near the exit leading to $t_{c-radial} \sim t_k$). Since the convective and conductive characteristic times are of the same order of magnitude either one can be compared against the device deformation time scale (t_d). Because near entrance of the tube it can be substantially higher than $t_{c-radial}$, in the following discussion we will utilize t_k as the characteristic thermal time scale.

The characteristic thermal time scale must be compared against the device deformation time scale (t_d) which, due to the periodic oscillations of our system, we set to one tube stretching-retraction period (i.e. one wave period). If the tube is stretched to ΔL (maximum of 64 mm) and the tube is actuated at rate L' , $t_d = 2\Delta L/L'$. In terms of the actuation angular frequency, ω , $t_d = 2\pi/\omega$. By adjusting the device actuation rate, we can vary t_d between 16 s and 300 s and explore regimes where $t_k/t_d \approx 1$ and $1 \gg t_k/t_d$. While our equipment limitations did not allow us to study the $t_k/t_d \gg 1$ regime, we will show later that it is not necessary in determining the limits of t_k/t_d where the quasi-static shape assumption is valid.

Thermofluidic characterization of the device operation

To evaluate the thermal behavior of the liquid-cooled soft tube we embedded a steel extension spring near the outer wall of the tube wall to act as both a joule heater and a resistive temperature probe. Specifically, by maintaining a constant 1.9A current through the spring while allowing the voltage to vary, during actuation we can measure both the heat generated ($\dot{Q}_{supply} = VI$) and the fluctuations in electrical resistance that are due to resistivity changes with temperature ($R = V/I$). Using the proportional relationship between electrical resistance and temperature (temperature coefficient for spring steel of $27 \text{ m}\Omega/^\circ\text{C}$), we can calculate the spatially-averaged spring (heater)

temperature (T_s). Out of the numerous variables that we measured, we found T_s provides the most sensitive metric to quantify cooling changes associated with stretching of the tube. We also considered other common performance variables including the heat removed by the cooling liquid, the overall heat transfer coefficient, the total thermal resistance, and the liquid Nusselt number (see ESI). However, we found that the impact of tube actuation on phase shift and amplitude change of these parameters is observable but comparable to the total experimental uncertainty. Conversely, the \bar{T}_s was measured using the carefully calibrated electrical resistance approach (see ESI), and thus, had a relatively smaller measurement uncertainty ($\pm 1.5^\circ\text{C}$). In addition, since it was the ‘furthest’ from the cooling fluid and inner wall undergoing shape change, \bar{T}_s demonstrated the most amplified effects of the tube actuation. In qualitative and static terms, the \bar{T}_s will be proportional to the thermal resistance between the heater and cooling water. Specifically, the point at which T_s is lowest will represent the point at which the thermal resistance posed by the wall and convection is lowest or, in other words, when the heater is most effectively cooled.

In Fig. 2 we present T_s results for tubes made out of only silicone (Fig.2a) and a 20% LM-silicone composite (Fig.2b). It is worth noting that for the same operating conditions in a silicone tube \bar{T}_s oscillates about $\sim 95^\circ\text{C}$ while for the liquid metal silicone composite it oscillates about substantially smaller $\sim 55^\circ\text{C}$. This demonstrates an improvement in the thermal performance of the device expected from the material transition to these more thermally conductive composites. To facilitate one-to-one comparison between the two materials, we plot the demeaned spring temperature, i.e. $\Delta T_s = T_s - \bar{T}_s$. Additionally, to clarify comparisons across the various stretch rates, the collected thermal data from each stretch rate was cyclically averaged across all studied oscillations and compiled into a single stretch-retraction cycle, converting time series data to periodic data (0 to 2π radians). Finally, for clear representation of the oscillatory nature of the

system, this averaged stretch-retraction cycle is simply repeated so that the plots in Fig. 2 range from 0 to 4π radians.

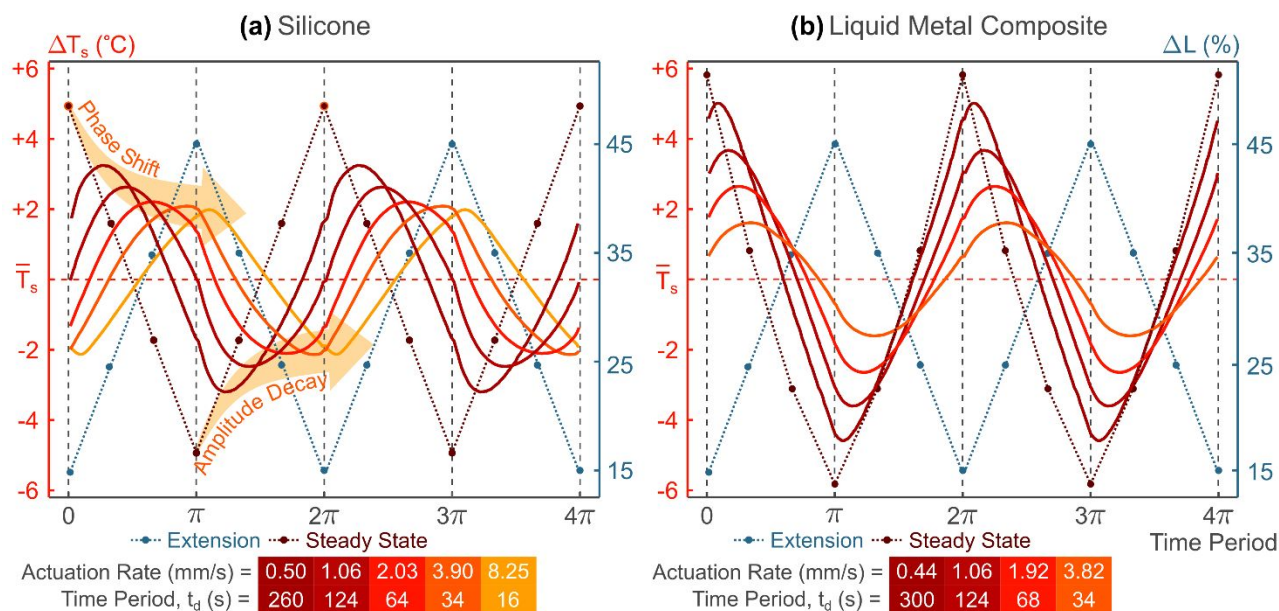


Fig. 2. Representative demeaned spring temperature over two cycles of extension-retraction for (a) a silicone tube with highlighting arrows to show the rate dependent phase shift and amplitude decay and (b) for a liquid metal composite tube consisting of 20% liquid metal volume fraction.

To set the baseline quasi-static predictions, we conducted steady state control experiments with fixed extensions (i.e. $t_d \rightarrow \infty$). As shown in Fig. 2, we studied steady-state behavior in tubes that were extended to 15%, 25%, 35% and 45% above the original length of about 254 mm (blue dots connected by dotted line that form a triangular wave). In our generalized representation, the corresponding ΔT_s that were measured during the non-actuated but stretched tube experiments also form a triangular wave that corresponds to ideal quasi-static behavior, indicated by the brown points connected by dashed lines in Fig. 2. Since at maximum extension (45%), the wall thickness

is at its minimum (0.82 mm) and the convective heat transfer surface area is at its maximum (23.7 cm²), the wall-cooling rate is at its maximum translating into lowest ΔT_s of -4.9°C for the silicone tube and -5.8°C for the composite tube. This value is 10°C to 12°C lower than ΔT_s measured for the lowest tube extension (15%), for which tube thickness is at its maximum (0.94 mm) and the convective heat transfer surface area is at its minimum (16.9 cm²).

When the tubes are actuated during operation, the ΔT_s deviates from the ideal quasi-static triangular wave in two ways. First, the amplitude of the oscillations decreases with increasing actuation rate. For example, for a silicone tube the static 15% extension results in a ΔT_s max of 4.9 °C but with actuation rates of 0.5 and 3.9 mms⁻¹ the maximum ΔT_s drops to 3.2 °C (-35%) and 2.1°C (-57%), respectively (see Fig.2a). For the composite tube the static 15% extension results in a ΔT_s of 5.8 °C but with actuation rates of 0.44 and 3.82 mms⁻¹ the maximum ΔT_s drops to 4.4°C (-24%) and 1.5 °C (-74%), respectively. Second, it is evident from Fig.2 that the deformation of the tube introduces a phase lag in ΔT_s that is proportional to the actuation rate. We discuss this phase shift (φ) in terms of π (radians) deviation from the quasi-static triangular wave. For example, for the silicone tube with actuation rates of 0.5 and 3.9 mms⁻¹ we measure a φ of 0.26π and 0.91π , respectively (see Fig.2a). For the composite tube with actuation rates of 0.44 mms⁻¹ and 3.82 mms⁻¹ there is a smaller φ of 0.09π and 0.34π , respectively. Consequently, our data shows that in all cases we have studied the thermal performance of the actuated soft thermal system departs from the static extension values. In other words, a quasi-static assumption based analysis would not be valid for the actuation rates that we were able to experimentally study with our setup. Next, we show that by re-evaluating the ΔT_s in terms of the previously discussed time scale ratio and considering a classical analytical model for an oscillating boundary condition problem,¹⁴ we can generally predict how slow actuation would have to be for the quasi-static assumption to be valid.

The characteristic time scale ratio and shape-modulation regimes

Fig.3a shows that the ΔT_s phase-shift data for silicone and composite tube actuation experiments both clearly decay with increasing device time scale (t_d). Furthermore, when presented as a function of the previously introduced conduction to device time scale ratio (t_k/t_d), the two data sets collapse into a single general curve that elucidates the role of the relative magnitudes of the characteristic time scales (Fig.3b). Specifically, our experiments cover φ data for t_k/t_d of about 0.6 down to 0.006. In the $t_k/t_d \approx 1$ regime, the over 1π phase shift results in a complete inversion of ΔT_s from the representative quasi-static behavior (i.e. T_s is heating up rather than cooling down when the tube is extending). As the t_k/t_d ratio decreases to 0.1, the phase-shift also decreases substantially to 0.25π . However, as the t_k/t_d ratio decreases even further the rate of φ decay decreases. With our most extreme measurement of t_k/t_d of 0.006 that corresponds to the slowest actuation (0.44 mms^{-1}) of the LM composite tube, the phase-shift decreases to 0.09π , representing a 9% temporal deviation. It is also evident from Fig.2b that this combination presents the closest actuated ΔT_s curve to the representative curve of the quasi-static assumption. Thus, while close, our experimental data still does not reach a regime in which the quasi-static assumption would be representative of our system behavior (defined here as a temporal deviation smaller than 2%). However, using a simple model that relates the time scales to the phase-shift and matches our data, we show that conditions under which this assumption is valid can be estimated.

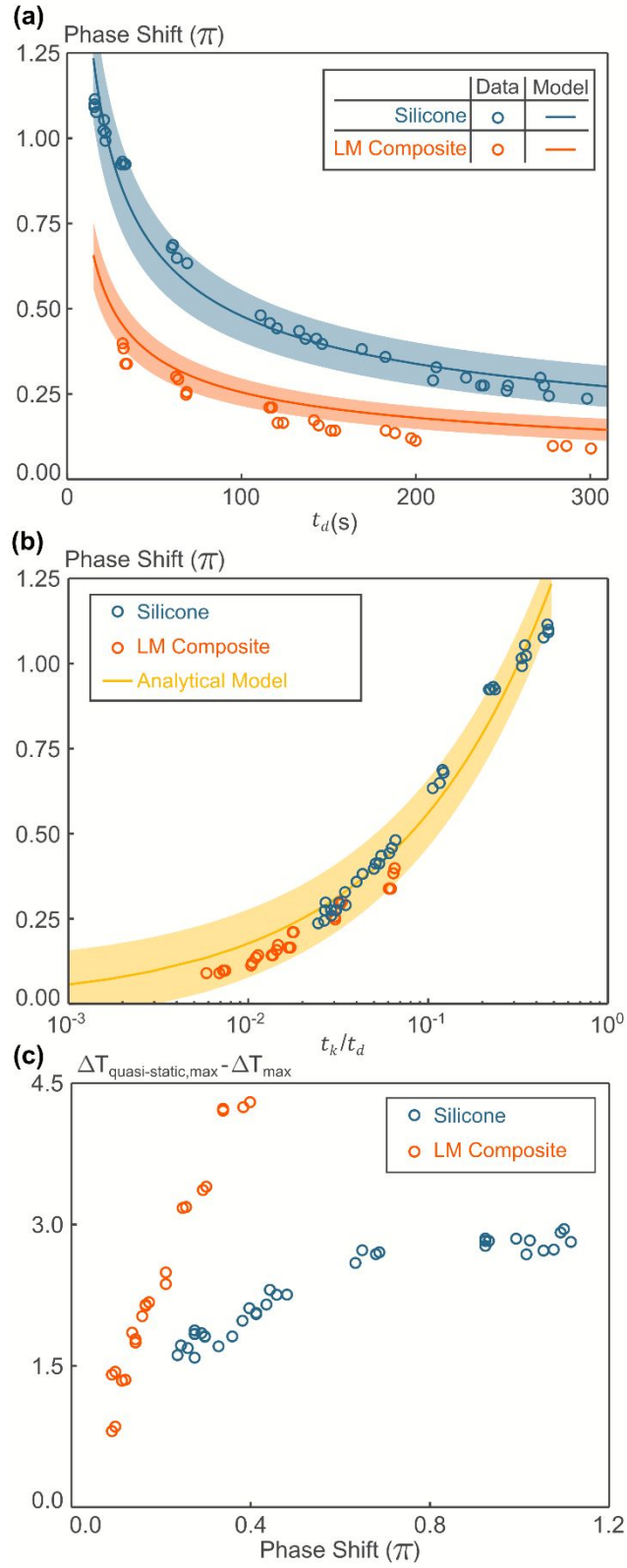


Fig. 3. The measured and theoretically predicted spring temperature phase shift as a function of (a) the device actuation time scale, t_d and (b) the dimensionless ratio of the conductive to device actuation time scale, t_k/t_d ; (c) the difference between peak average spring temperature in non-actuated (quasi-static like) and actuated conditions as a function of the corresponding phase-shift.

We can gain insight into the transient aspects of heat transfer processes occurring during our soft device operation by exploring the functional forms of solutions to heat transfer problems with periodic thermal perturbations. For example, the transient component of the analytical solution for the temperature profile of a semi-infinite medium undergoing periodic temperature fluctuations at the wall boundary is $\cos(\omega t - Kx)$.¹⁴ In this formulation, x is the relevant length (in case of the semi-infinite problem distance away from the thermally oscillating surface), ω is the angular frequency of thermal oscillations, and K (m^{-1}) is the wave number that is defined as $(\omega/2\alpha)^{1/2}$. By manipulating the previously introduced definitions of the time scales we obtain $\omega = 2\pi/t_d$ and $\alpha = x^2/t_k$. By substituting these relations and employing the wall thickness for the characteristic length (i.e. $x = h$ or the distance from the spring, where we measure the temperature, to the inner diameter of the tube), we obtain an expression for the phase-shift ($\varphi = Kx$) in terms of the characteristic time scale ratio, t_k/t_d :

$$\varphi = Kx = Kh = \left(\frac{t_k}{t_d} \right)^{1/2}$$

As shown in Fig. 3b, when the variation in h and α is taken into account (see discussion below), this simple relationship provides an excellent prediction of the measured phase-shift data. In other words we can, with confidence, use this simple relationship to extrapolate the data and determine the value of φ at $t_k/t_d < 0.006$. For example, for t_k/t_d of 10^{-3} we can expect a very small φ of

0.015π that can be considered negligible (below 2% of the time-period). If we also take into account that the difference between ΔT_s maximums for the quasi-static curve and the actuated curves decreases with φ (see Fig.3c), using linear extrapolation we can estimate that t_k/t_d of 10^{-3} the ΔT_s will be within 0.25°C of static values. Consequently, we assert that t_k/t_d of 10^{-3} sets an appropriate threshold for the gradual shape modulation regime ($t_k/t_d \ll 1$), where the quasi-static shape assumption is appropriate. If t_k/t_d is greater than this value, the device will operate in a ‘rapid’ shape modulation regime where transient shape effects must be taken into account to capture the transient behavior of the system.

While our equipment limitations did not allow us to experimentally probe the regime of $t_k/t_d \gg 1$, the increasing phase shift and decreasing amplitude trends observed in Fig.2 and Fig.3 suggest that eventually the magnitude of oscillation might saturate and, for more thermally conductive tubes, even flatten out (i.e. the concept of a phase-shift would no longer be applicable). However, in this very rapid shape modulation regime other phenomena are likely to have a more significant impact on the soft system performance because the device actuation time scales will become smaller than the heat transfer time scales (≈ 1 to 2 s). The behavior of soft systems in this regime presents an interesting area for future exploration and could warrant an analysis encapsulating three or more time scales.

Lastly, we discuss the impact of LM micro-droplet shape transition brought about by tube extension, that is evident in images in Fig.1c, which imparts anisotropy to the composite thermal properties. This temporal micro-structure change will introduce associated temporal variations in α and, in turn, t_k . While the directionality of α in LM composites under strain has not been explicitly studied, it is likely to be proportional to the changes in thermal conductivity since diffusivity is defined as $\alpha = k/\rho c$ (where density ρ and specific heat c are compositional values

and should not be impacted by mechanical deformation). Bartlett et al.⁴ demonstrated that along the direction of stretch in a rectangular slab, thermal conductivity increases by up to five fold. For heat transfer from the spring to the cooling water, it is the transverse thermal conductivity that is relevant (in the plane normal to the axis of the stretched LM droplets in Fig.1c). This value, $k_{transverse}$, is commonly evaluated from the geometric mean of the conductivity in the associated two axes, which if you consider this problem from an axisymmetric perspective, the transverse plane will consist of the radial (r) and axial (z) axes and so, $k_{transverse} = \sqrt{k_r k_z}$.⁴ Using approximated values from Bartlett et al.,⁴ we estimate that with the 45% extension of the LM composite tube the transverse α will increase from $0.34 \text{ mm}^2\text{s}^{-1}$ that was measured at 0% extension to $0.46 \text{ mm}^2\text{s}^{-1}$ (vs. $0.13 \text{ mm}^2\text{s}^{-1}$ for the silicone matrix). In fact, we speculate that the α increase could potentially be even higher due to the particle deformation in the θ direction as well (see Fig.1c). While thorough validation of these values is beyond the scope of the current work, the fact that in Fig.3 most experimental data is captured by the model envelope for which we used a α of $0.46 \text{ mm}^2\text{s}^{-1}$ for t_k and the potential for the remaining deviation to be met by a further increase in diffusivity, suggest merit to our analysis.

Conclusions

We used liquid metal and silicone composites to develop an elementary thermofluidic system consisting of a soft, heat generating pipe that is internally cooled with flow of water and analyzed its thermal behavior as it underwent periodic stretching and retraction at varying frequencies during its operation. Our experiments revealed that, as compared to values collected from stretched but stationary tubes, actuation causes a decrease of the peak amplitude and causes a phase-shift (φ) in the spatially-averaged spring temperature (which we found to be a highly sensitive metric of

our system transient behavior). This phase-lag can be extensive, even causing full inversion of the ΔT_s from that representative of the quasi-static behavior. When analyzed in terms of the ratio of conduction to device actuation time scales (t_k/t_d), all our φ data collapsed into a single general curve. By recasting the wave number in terms of time scales in the classical analytical solution to heat transfer in semi-infinite medium with thermally oscillating boundary condition, we showed that this general curve follows the derived $\varphi = (\pi t_k/t_d)^{1/2}$ relationship. This analysis and our experiments show that our soft thermofluidic system behavior can be predicted with under a 2% temporal deviation (φ) from static extension behavior for a t_k/t_d ratio lower than about 10^{-3} (can be thought of as quantification of the $t_k/t_d \ll 1$ condition). As such, we termed this conditions the gradual shape modulation regime. In contrast, when the t_k/t_d ratio increases above 10^{-3} the device behavior analysis based on quasi-static shape assumptions would provide an increasingly poor prediction of the system, thus we termed these conditions the rapid shape modulation regime. In this regime, the transient shape effects must be taken into account for accurate system modeling. While our equipment limitations did not allow us to experimentally probe the regime of $t_k/t_d \gg 1$, our data suggests that eventually the magnitude of oscillation might saturate and, for more thermally conductive tubes, even flatten out. However, in this very rapid shape modulation regime other phenomena are likely to have a significant impact on the soft thermofluidic system performance, which presents an interesting area for future exploration. Although developed here for an elementary soft thermofluidic system, our timescale analysis should provide a general framework for the analysis of soft thermal systems such as heat exchangers that undergo shape change during operation. Some applications for such devices are already starting to emerge in diverse areas that include personal cooling garments,^{15,16} soft robotics for medical applications,¹⁷ cooling for high powered robotics,^{18,19} corrosion resistant applications,²⁰ HVAC,²¹ flexible

stretchable heating,^{22–24} and fog harvesting.²⁵ Furthermore, the ease of multimaterial manufacturing stemming from innovations in 3D printing²⁶ combined with future enhancements in thermo-mechanical aspects of soft materials will enable many novel soft thermal systems to emerge and potentially outperform their rigid analogues. As such, we hope that this work will facilitate their development by providing a starting point for their thermal design.

Experimental

Soft, heat generating tube fabrication

The composites were fabricated by dispersing the filler particles in a two-component silicone (SmoothOn, SortaClear 14 A and B). In this study, we used a liquid metal filler particles which were fabricated by high-speed shear mixing liquid metal eutectic GaInSn, prepared in house (Ga 68%, In 22%, Sn 10%, all obtained from RotoMetals), in an ethanol solution until the desired particle distribution with an average of about 60 μm was achieved (see ESI for details). Once the appropriate particle distribution was achieved, we removed as much of the ethanol from the top as possible with the use of a syringe while maintaining enough to ensure the liquid metal suspension did not re-coalesce. We then mixed the filler particles into the silicone component A with the use of a high-speed mixer (Dremel 3000) to ensure even dispersions and then further mixed with the silicone component B. The final mixture was then degassed in a vacuum chamber to remove air that was incorporated in the mixing process and any remaining ethanol. Finally, the mixtures were injection cast at a rate of 0.5 mlmin^{-1} into molds consisting of vertically hung glass tubes (McMaster # 8729K33, 5.59 mm inner diameter) with a centered nylon line (Catch All Tackle sku:2519933, 1.9 mm diameter under tension) kept under a constant tension along the tube axis, and an extension spring (McMaster #9664K74, 3.96 mm inner diameter) stretched to 275 mm (see

ESI for further details). The pre-extension of the spring allowed for the composite mixture to flow into the gaps between the coils and ensured that there was no electrical short between neighboring spring coils. Due to difference between the glass tube inner diameter and the spring outer diameter and its pre-extension, a layer of the silicone mixture forms around the coil, effectively embedding a stretchable joule heater in the tube wall. The final mold was then hung under a constant tension and allowed to cure for 16 hours at lab temperatures 18 to 20°C. Post cure, with the use of isopropanol alcohol we extract the prototypes and formed electrical leads at both ends of the device by exposing and unravelling parts of the spring coil. We note that we also fabricated tubes with composites with higher content of LM (30-50%), however, we found that these materials were leaking liquid metal as well as water through pinholes during operation.

Thermal Characterization

The thermal conductivity of the materials were measured using a Hot Disk Thermal Constants Analyzer (Thermtest, TPS2500S). To satisfy the infinite sample assumption underlying this method, it is recommended that the thermal wave probing depth be smaller than the smallest sample dimension, calculated as $\Delta_p = 2\sqrt{\alpha t}$, where α is thermal diffusivity of the sample and t is the run time of the experiment. Based on previous experiments, it was estimated that for these materials the maximum $\Delta_p \approx 6$ mm.⁹ Consequently, 10 mm thick disks with 25 mm diameter were cast. Three sets of samples for the silicone and 20% liquid metal composite were fabricated and tested. The measurements using sensor design 5465 (3.2 mm radius Kapton sensor) were carried out, with a measuring time of 20 s and a heat flux of 50 and 80 mW for the silicone and composite, respectively. In this test method, the heat sensor was used as both a heat source and a temperature sensor and thus measured both the heat input, output, and the temperature increase in the sensor.

Using this transient data, the hot disk iteratively calculated the thermal conductivity and thermal diffusivity values with a manufacturer specified accuracy of $\pm 5\%$.

Testing Procedure

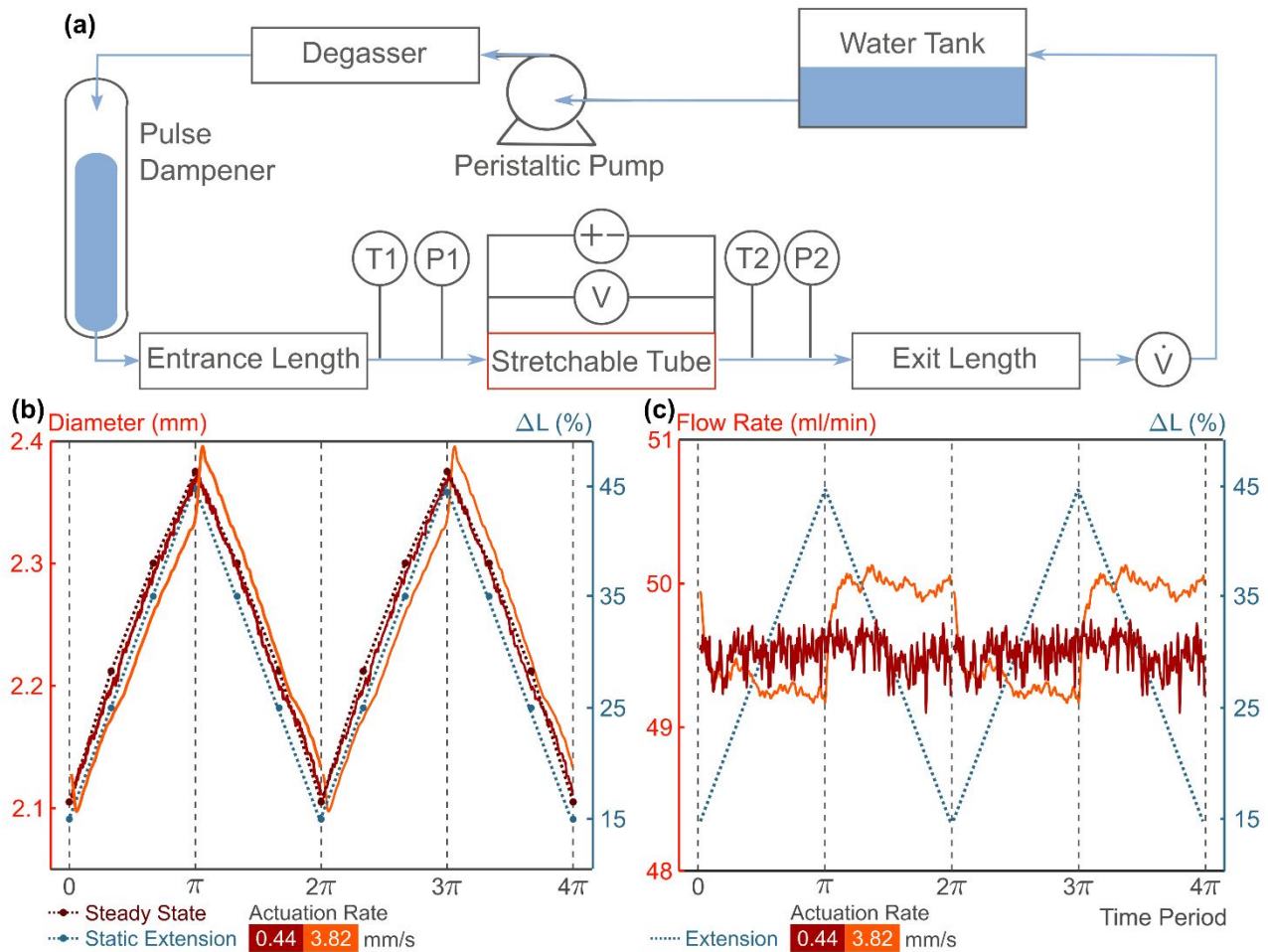


Fig.4. (a) An illustration of the flow loop that was implemented in this study, (b) the effect of stretch-retraction of the tube on its inner diameter with a static extension, a slow actuation rate of 0.44 mms^{-1} , and a fast actuation rate of 3.82 mms^{-1} , and (c) the effect of stretch-retraction on the flow rate through the device.

To explore the thermal performance of the stretchable devices, we developed the flow loop illustrated in Fig.4a. We set the inlet temperature to 10°C to ensure minimal thermal degradation and thermal expansion of the composite, the importance of which is discussed later, by using a temperature-controlled circulating water bath (45 L version from VWR). The cooling water was pumped at a constant flow with the use of a peristaltic pump (OMEGA FPU500) and, in order to ensure a constant laminar flow into the stretchable device, the flow was fed into a custom-built pulse dampener. Prior to entering the test section, the flow was fully developed hydrodynamically with the use of an entrance length of the same inner diameter as the devices, $D = 1.9$ mm, and a length of 300 mm which is well above the recommended length of $50D$ the inner diameter obtained from the $0.05ReD$ expression (Re corresponds to the Reynolds number).¹² To prevent any hydrodynamic exit effects, an exit length identical to the entrance length was fitted after the test section. We note that the identified regimes should be applicable to a device that is cooled by turbulent flow since all convective time scales would be substantially decreased providing the $t_k \gg t_c$ condition. The flow from the device was monitored and recorded with the use of an inline flow sensor (OMEGA FLR1007) after the exit length, from where the cooling water was recirculated back to the water bath. The test section itself was fitted with a prototype device which was heated by running a constant current of 1.9A through the spring coil. The device, during operation, was linearly and periodically stretched in a tensile fashion from an initial 15% stretch, that was chosen to avoid any tube sagging, to up to 45% over the original tube length at multiple rates, ranging from 0.3 - 8 mm/s, with the use of linear actuators (Firgelli Feedback Rod Linear Actuators with 20 cm extension and 200 lbs capability, see ESI for further information). Finally, the test sections external environment was controlled with use of flexible insulation in the form of

cotton frills that were hung from the containment ceiling. The frills were used to ensure a high, constant thermal resistance to the environment, independent of stretch rate.

The testing procedure consisted of allowing the flow to reach a steady state of 50 mlmin^{-1} , and then heating the device via the joule heater. Once the ambient temperature measured directly above the tube did not vary more than $\pm 0.5^\circ\text{C}$ over 10 minutes, steady-state was achieved and the device was actuated. For each stretch rate, a 10 minute initiation period was followed by 20 minutes of data collection. In between individual stretch experiments, at least a 2 minute unperturbed period in which flow achieved steady state was introduced. During testing the pressure drop (OMEGA PX2300-1DI), temperature difference (PTC10 with T-type thermocouples), the voltage across the test device, the length/extension (via the in-built potentiometer in the actuator), and flow rate were measured at a frequency of 4 Hz. For each tube composition and extension rate, experiments were repeated four times. In addition, we conducted control experiments with fixed tube extension of 15, 25, 35, and 45%.

Experimental Considerations and Raw Data Analysis

By nature of this system, we observed a coupling of mechanical, thermal, and fluid properties, which we outline individually below. Concerning the mechanics of deformation, the tube mechanics are dominated by the steel spring embedded in the device wall. Due to the pseudo outer-wall constraint imposed by this spring, when extended the tube inner diameter expands instead of contracting. From experimental characterization, we found this behavior to be in between a tube that is mechanically unconstrained and fully constrained at its outer-wall (see ESI for further discussion). To overcome this complex nature of tube deformation and to account for other effects induced by rate of stretching or thermal changes, we back-calculated the inner diameter of the tube

from the measured pressure drop using the Hagen-Poiseuille law for pressure drop across a pipe with laminar flow:¹²

$$\Delta P = - \frac{128\mu\dot{V}L}{\pi D^4}$$

Where, ΔP is the pressure drop across the test section, μ is the viscosity of water at a mean fluid temperature between the inlet and outlet, \dot{V} is the flow rate, and L is the length of the test section. By measuring each of these variables during actuation, we calculate the inner diameter of the tube also during actuation, as illustrated in Fig.4b. Since the steel extension spring does not constrict during extension, we are also able to calculate the wall thickness between the spring (constant inner diameter of 4 mm) and the tube inner wall, which is the characteristic conduction heat transfer length used to calculate t_k . We observed that diameter deformation is most drastic in the first 15% of extension, after which rate of change with extension slows down. As noted previously, to avoid any sagging effects, our extension ranged from 15% to 45% of the original length. Finally, we note a weak coupled effect between the wall temperature and the tube mechanics stemming from thermal expansion of the material. In our exploratory experiments, we ran 2A of current through the test devices and observed spring temperatures of up to 120°C and a deviation of diameter by up to 6% of the expected value. To mitigate these effects, we reduced the spring temperature by reducing the current to 1.9A and by running colder water maintained at 10°C at the inlet.

With regards to the hydrodynamics, in order to ensure accurate predictions through the Hagen-Poiseuille law, we maintained laminar flow by ensuring a Re below 500 for all tube extension states. We achieved this with the use of a small inner diameter combined with a low inlet temperature (10°C), to increase viscosity, and a low flow rate (50 mlmin⁻¹). Furthermore, in the work by Kumaran et al²⁷⁻²⁹, a hydro-mechanical relation between the shear modulus of the tube

and turbulence transition Re number was highlighted (i.e. softer tubes promote transition to turbulence). Kumaran also quantified the extent of tube inflation, by drawing a correlation between material softness and the Re number. By using a silicone matrix with a shear modulus of ~ 50 kPa and $Re < 500$, we stayed below the lowest transition point of $Re \approx 500$ (reported for a soft gel-silicone with a shear modulus of ~ 18 kPa), and ensured negligible tube inflation due to flow.²⁹ Thus, with these considerations, we ensured minimal effects of fluid dynamics on the system. In other words, the cooling fluid acted as a thermal sink for the heat generated by the spring and provided means of quantifying the inner diameter during operation.

Finally, though we isolated the tube mechanics from the hydrodynamics, we note that there is a coupled effect of the tube mechanics on the fluid flow in the form of a pumping effect caused by periodic expansion-contraction that creates flow fluctuations proportional to the rate of actuation. This effect can be clearly seen in Fig.4c where, at an actuation rate of 4 mms^{-1} , the flow takes on a square wave profile. In our exploratory experiments, we found this profile eventually becomes sinusoidal in nature if the rate is increased further. However, these flow oscillations induced by the tube actuation only occur at higher actuation rates and are below 5 mlmin^{-1} (i.e. 10% of used flow rate) in the range of actuation rates that we report data for, thus can be neglected.

To quantify the thermal performance of the devices, we evaluated the spatially averaged spring temperature. To do so, we measured the electrical resistance of the spring coils, embedded in silicone, as a function of temperature in a combination of water and silicone oil baths to achieve a wide range of temperature calibrations points. By doing so, we evaluated the temperature coefficient (γ) of our spring to be $0.0272 \text{ } \Omega/\text{ }^\circ\text{C}$, which matches other previously reported values for steel³⁰ (see ESI for further information). Finally, a reference temperature, T_{ref} , of about $73 \text{ }^\circ\text{C}$ was chosen to minimize the deviation that the linearization of the temperature resistance curve

could cause. The resistance of each tube at a similar temperature was measured by submerging the tube in a homogenous, constant temperature water bath and used as the reference resistance, R_{ref} . To calculate average spring temperature, T_s , from the measured spring resistance, R_{spring} , at other conditions we used the following equation:

$$T_s = T_{ref} + \frac{R_{ref} - R_{spring}}{\gamma}$$

We ensured that the majority of generated joule heating within coil ($\dot{Q}_{supply} = VI$) was removed by the cooling water by comparing it with the heat removed by the water. We calculated the total heat transfer rate to the cooling water, \dot{Q}_{water} , using the following equation:¹²

$$\dot{Q}_{water} = \dot{m}c_p(T_{m,out} - T_{m,in})$$

Where \dot{m} is the flow rate, which is set to 0.8 gs^{-1} (50 mlmin^{-1}), $T_{m,in}$ and $T_{m,out}$ are the mean inlet and outlet water temperatures, and c_p is the specific heat taken as $4184 \text{ J/kg}^\circ\text{C}$. The current supply was kept constant (1.9A) and the voltage across the device was actively collected. By comparing the \dot{Q}_{supply} to \dot{Q}_{in} , we evaluated the effectiveness of insulation and it was found to minimize heat loss to air down to 10% of the \dot{Q}_{supply} (see ESI for further details).

Conflicts of interest

There are no conflicts to declare.

Acknowledgements

The authors gratefully acknowledge funding from the National Science Foundation through award number CBET #1724452.

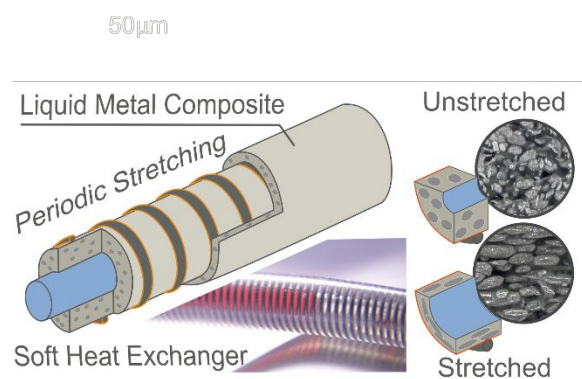
Notes and references

- 1 R. K. Shah and D. P. Sekulic, *Fundamentals of heat exchanger design*, John Wiley & Sons, 1st edn., 2003.
- 2 E. H. Wissler, *Human Temperature Control: A quantitative Approach*, Springer, Berlin, Germany, 1st edn., 2018.
- 3 A. Fassler and C. Majidi, *Adv. Mater.*, 2015, **27**, 1928–1932.
- 4 M. D. Bartlett and C. Majidi, *Proc. Natl. Acad. Sci.*, 2017, 8–15.
- 5 R. Tutika, S. H. Zhou, R. E. Napolitano and M. D. Bartlett, *Adv. Funct. Mater.*, 2018, 1804336.
- 6 E. J. Markvicka, M. D. Bartlett, X. Huang and C. Majidi, *Nat. Mater.*, 2018, **17**, 618.
- 7 J. Tang, X. Zhao, J. Li, R. Guo, Y. Zhou and J. Liu, *ACS Appl. Mater. Interfaces*.
- 8 W. Kong, Z. Wang, M. Wang, K. C. Manning, A. Uppal, M. D. Green, R. Y. Wang and K. Rykaczewski, *Adv. Mater.*, 2019, **31**, 1904309.
- 9 M. I. M. Ralphs, N. Kemme, P. B. Vartak, E. Joseph, S. Tipnis, S. Turnage, K. N. Solanki, R. Y. R. Y. Wang and K. Rykaczewski, *ACS Appl. Mater. Interfaces*, 2018, **10**, 2083–2092.
- 10 M. Ralphs, W. Kong, R. Y. Wang and K. Rykaczewski, *Adv. Mater. Interfaces*, 2019, **1801857**, 6.
- 11 A. Uppal, M. Ralphs, W. Kong, M. Hart, K. Rykaczewski and R. Y. Wang, *ACS Appl. Mater. Interfaces*, 2020, **12**, 2625–2633.

- 12 T. L. Bergman, A. S. Lavine, F. P. Incropera and D. P. Dewitt, *Fundamentals of heat and mass transfer*, John Wiley & Sons, Inc, New York, 2011.
- 13 A. Bejan, *Convection heat transfer*, John wiley & sons, 2013.
- 14 H. S. Carslaw and J. C. Jaeger, *Heat conduction in solids*, Oxford Univ. Press, Cambridge, 1st edn., 1959.
- 15 P. Kotagama, A. Phadnis, K. C. Manning and K. Rykaczewski, *Adv. Mater. Technol.*
- 16 A. D. Flouris and S. S. Cheung, *Ann. Biomed. Eng.*, 2006, **34**, 359–372.
- 17 J. P. D. Shing Shin Cheng,* , Yeongjin Kim, *IEEE Trans Robot.*, 2018, **33**, 986–993.
- 18 D. Kim, J. Ahn, O. Campbell, N. Paine and L. Sentis, *IEEE/ASME Trans. Mechatronics*, 2018, 1–11.
- 19 D. Kim, O. Campbell, J. Ahn, L. Sentis and N. Paine, in *Humanoid Robotics (Humanoids)*, 2017 IEEE-RAS 17th International Conference on, IEEE, 2017, pp. 710–717.
- 20 J. G. Cevallos, A. E. Bergles, A. Bar-Cohen, P. Rodgers and S. K. Gupta, *Heat Transf. Eng.*, 2012, **33**, 1075–1093.
- 21 C. T’Joen, Y. Park, Q. Wang, A. Sommers, X. Han and A. Jacobi, *Int. J. Refrig.*, 2009, 32, 763–779.
- 22 N. S. Jang, K. H. Kim, S. H. Ha, S. H. Jung, H. M. Lee and J. M. Kim, *ACS Appl. Mater. Interfaces*, 2017, **9**, 19612–19621.

- 23 J. Jang, B. G. Hyun, S. Ji, E. Cho, B. W. An, W. H. Cheong and J.-U. Park, *NPG Asia Mater.*, 2017, **9**, e432–e432.
- 24 K. Rykaczewski, *Temperature*, 2019, **6**, 97–100.
- 25 Q. Zhang, G. Lin and J. Yin, *Soft Matter*, 2018, **14**, 8276–8283.
- 26 M. A. Skylar-Scott, J. Mueller, C. W. Visser and J. A. Lewis, *Nature*, 2019, **575**, 330–335.
- 27 V. Kumaran, *Sadhana - Acad. Proc. Eng. Sci.*, 2015, **40**, 911–923.
- 28 M. K. S. Verma and V. Kumaran, *J. Fluid Mech.*, 2012, **705**, 322–347.
- 29 M. K. S. Verma and V. Kumaran, *Phys. Rev. E - Stat. Nonlinear, Soft Matter Phys.*, 2015, **91**, 1–15.
- 30 All About Circuits, <https://www.allaboutcircuits.com>.

Table of Contents



The behaviour of a soft thermofluidic system, made of a liquid metal silicone composite, undergoing large scale transient stretching is studied. With a time scale analysis, transient regimes and the limits of quasi-static assumptions are explored.